Synthesis of High Purity Silicon Nanoparticles in a Low Pressure Microwave Reactor

Jörg Knipping,[a] Hartmut Wiggers,[a] Bernd Rellinghaus,[a] Paul Roth,[a, *] Denan Konjhodzic,[b] and Cedrik Meier[b]

[a] *Institut für Verbrennung und Gasdynamik, Universität Duisburg-Essen, D-47048 Duisburg, Germany*
[b] *Laboratorium für Festkörperphysik, Universität Duisburg-Essen, D-47048 Duisburg, Germany*

The formation of pure single crystalline silicon nanoparticles by microwave induced decomposition of silane in a low pressure flow reactor is reported. The morphology and crystal structure of the particles are characterized *in situ* by particle mass spectrometry (PMS) and *ex situ* by means of X-ray diffraction, high resolution transmission electron microscopy, electron energy loss spectroscopy, and infrared spectroscopy. The preparation method allows for the adjustment of the mean particle diameter in the range 6 nm $\leq d_{PM} \leq$ 11 nm by controlling the precursor concentration, gas pressure, and microwave power. Spectroscopic investigations reveal that the particles are single crystal silicon. The potential on *n*- or *p*-type doping is in progress.

Keywords: Silicon, Nanoparticles, Microwave Plasma, Low-Pressure Flame, HRTEM, EELS, FTIR, XRD.

RESEARCH ARTICLE

1. INTRODUCTION

In the early 1990s, a widening of the electronic band gap due to quantum size effects and the existence of photoluminescence in the visible range of the electromagnetic spectrum (vis-PL) at room temperature has been discovered in (meso)porous and nanocrystalline silicon.[1–3] Since then, the research in this type of material has gained enormous attention. Cullis and Canham[4] have demonstrated that inclusions of nano*crystalline* silicon (nc-Si) within the porous silicon matrix are responsible for the occurrence of vis-PL. In recent years, detailed investigations have proven a distinct dependence of the width of the band gap ΔE and the PL on the silicon crystallite size.[5–8] As for possible technical applications, it has been shown that photo- and electroluminescence in the visible can be obtained by building electrode structures that contain nc-Si.[9] Martínez-Duart and Martín-Palma[10] have reviewed the potential of using porous silicon in applications such as LEDs, photodetectors and solar cells.

A variety of methods have been employed to prepare nc-Si and Si nanoparticles. The most prominent of these methods include gas-phase based techniques, such as thermal evaporation of Si or SiO, laser induced and thermal pyrolysis of silane, or plasma enhanced chemical vapour deposition (PECVD).[5, 6, 11–16] Among these, plasma based processes provide the advantage of a reduced risk of contaminations, e.g., those mediated by the contact with hot surfaces in hot-wall reactors. The particle morphology and the crystal structure depend sensitively on the details of the preparation, and one can produce amorphous, single crystal and even coated particles, which consist of a crystalline Si core surrounded by an amorphous oxide shell. The morphological and structural details are of significant importance, since they immediately affect the physical properties of the particles. For example, it has been shown that an amorphous oxide environment in the form of a matrix or a shell imposes a size dependent change of the lattice parameters on the crystalline Si nanoparticles.[16] Such stress induced modifications of the crystal structure and the chemical modification of the particle surface are considered responsible for changes in both the width of the band gap and the photoluminescence.[17] And, in Si quantum dots, Si/SiO_2 interfaces have been demonstrated to enhance the optical gain in light amplification applications significantly.[18]

In the present paper, experiments on the synthesis of silicon nanoparticles in a microwave induced low pressure flow reactor are reported. In general, the experimental setup is scalable to industrial dimensions and, thus, provides the potential for mass production. Although similar preparation methods are already introduced in the literature, the obtained Si particles are usually embedded in either polysilane or silica matrices[3, 14, 15] and the methods provide no control of the particle size.[14, 15] Therefore, particular attention is

*Author to whom correspondence should be addressed.

  1533-4880/2004/04/1039/006/$17.00+.25 doi:10.1166/jnn.2004.149

paid to the influence of the precursor concentration, the gas pressure and the supplied microwave power on the particle.

2. EXPERIMENTAL DETAILS

Silicon nanoparticles were prepared by microwave induced electrical discharge dissociation of silane (SiH_4) in a low pressure flow reactor. The experimental setup is schematically depicted in Fig. 1. The reactor consists mainly of a quartz glass flow tube into which the premixed reaction and dilution gases (SiH_4, H_2, Ar) are injected. The microwave energy is coupled into the gas flow forming a flame-like plasma torch. The plasma zone extends 2 cm in diameter and, depending on the gas velocity and the applied microwave power, has an axial length of 5 cm to 20 cm. The microwave generator is driven at a frequency of $f_{\mu W}$ = 2.45 GHz and the maximum microwave power is $P_{\mu W}$ = 2000 W. Within the experiments reported here, we have varied the microwave power in the range 300 W $\leq P_{\mu W} \leq$ 550 W. The total gas pressure was limited of 20 mbar $\leq p \leq$ 50 mbar and the SiH_4 precursor concentration was varied in the range 1061 ppm $\leq$ c(SiH_4) $\leq$ 4068 ppm. The generated particles were separated from the exhaust gases by a molecular beam system and collected on a surface. Alternatively, filter sampling of particles was employed.

The particle size was measured *in situ* using a particle mass spectrometer (PMS).[19] Additional *ex situ* sizing has been carried out by means of BET gas adsorption. Assuming solid, spherical and monodisperse particles, the specific surface area σ is related to the particle diameter d_P according to $d_P(\mathrm{BET}) = 6000/(\rho\sigma)$, where ρ denotes the particle density. For the structural characterization of the particles, X-ray diffraction (XRD) and high resolution transmission electron microscopy (HRTEM) have been employed. The XRD investigations have been conducted in conventional $\Theta - 2\Theta$ geometry using CuK_α radiation (λ = 0.15406 nm). For HRTEM, we have used a Philips Tecnai F20 microscope (200 kV, field emission gun) equipped with a Gatan image filter (GIF 2000) for electron energy loss spectroscopy (EELS). Fourier transform infrared (FTIR) spectra in the mid infrared range (MIR, wave number range 500 $cm^{-1} \leq k \leq$ 5000 cm^{-1}) have been measured in a vacuum spectrometer utilizing a mercury cadmium telluride (MCT) detector.

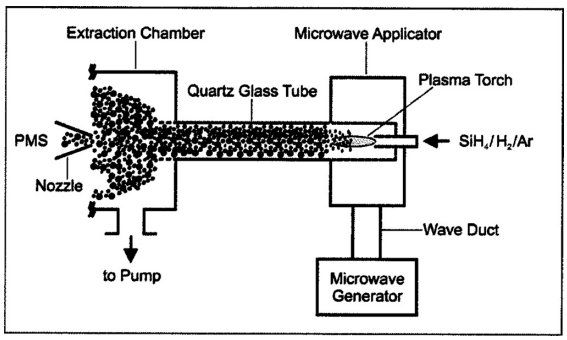

Fig. 1. Schematic drawing of the experimental setup for the preparation of Si nanoparticles. The main components are (in downstream sequence): Gas inlet. Microwave system consisting of the microwave generator, the wave duct and the microwave applicator. Quartz glass tube. Particle extraction chamber with particle mass spectrometer (PMS) and pumping system.

3. RESULTS AND DISCUSSION

3.1. Particle Mass Spectrometry (PMS)

The size distribution of the Si particles produced in the microwave induced plasma flow has been measured by particle mass spectrometry (PMS). Examples showing the probability density function (PDF) of the particle size for various flow conditions are shown in Figs. 2 to 4. The parameter in Fig. 2 is the initial SiH_4 concentration varying from 2120 ppm to 4060 ppm. As expected, the mean particle diameter derived from a fit of a log-normal size distribution function[20] to the experimental data increases from d_{PM} = 7 nm to d_{PM} = 10 nm with increasing precursor concentration, and also the geometrical standard deviation becomes larger. The pressure effect, see Fig. 3, is also significant. In this case, the broadening of the size PDF for p = 30 mbar is obvious. In general, the mean particle sizes, as determined from PMS, are found to be in good agreement with the results of BET measurements.

The effect of the microwave power coupled into the plasma flow on the particle size distribution function is illustrated in Fig. 4. With increasing power, the mean size of the Si particles decreases. This might be surprising at the first glance, since higher microwave power means higher plasma temperature, which in turn should result in a more effective electrical discharge dissociation of the SiH_4. However, such

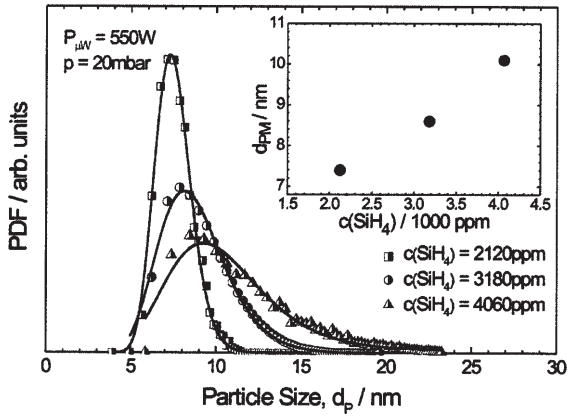

Fig. 2. Influence of the precursor concentration of silane, c(SiH_4), on the particle size distribution, as determined by particle mass spectrometry. The microwave power and total gas pressure are $P_{\mu W}$ = 550 W and p = 20 mbar, respectively. The insert shows the resulting mean particle size d_{PM} as a function of c(SiH_4).

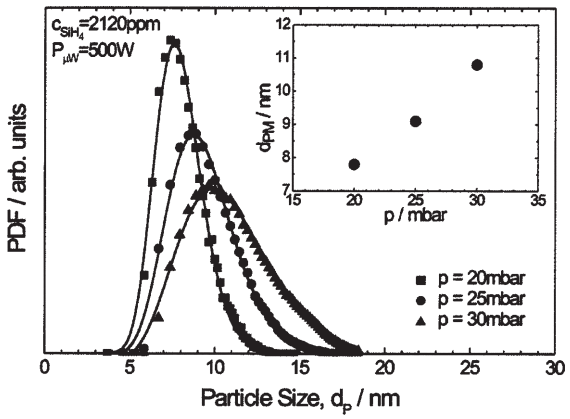

Fig. 3. Influence of the total gas pressure, p, on the particle size distribution, as determined by particle mass spectrometry. The precursor concentration of silane and the microwave power are c(SiH_4) = 2123 ppm and $P_{\mu W}$ = 500 W, respectively. The insert shows the resulting mean particle size d_{PM} as a function of p.

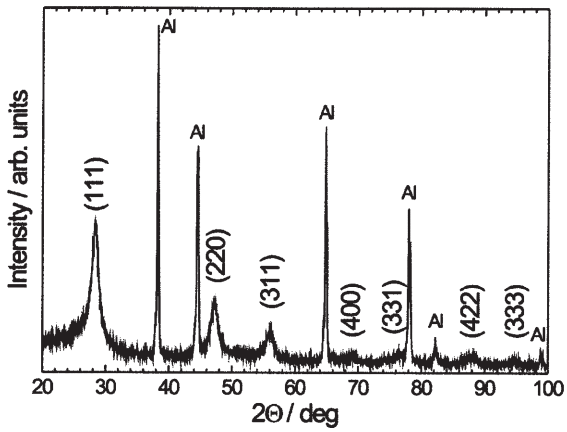

Fig. 5. XRD pattern of Si nanoparticles with a BET diameter of d_P(BET) = 5 nm, as obtained by using Cu k_α radiation (λ = 0.15406 nm). The Bragg peaks are labelled by their Miller indices. Peaks labelled "A1" originate from the aluminium substrate.

high power also leads to an increased charging of both the gaseous species and the particles and, thereby, to increased repulsive forces between the primary particles, whose collisional growth is thereby reduced. Apparently, a combination of both effects results in a favoured formation of very small particles.

3.2. X-Ray Diffraction (XRD)

In Fig. 5, an XRD pattern of particles prepared at conditions p = 50 mbar, c(SiH_4) = 1000 ppm and $P_{\mu W}$ = 300 W is shown. From BET measurements, the particle size was determined to be d_P(BET) ≅ 5 nm. Except for the peaks arising from the aluminium substrate, all occurring Bragg peaks are attributed to elementary silicon. After calibrating the pattern with respect to the known positions of the Al Bragg peaks, the lattice constant of the Si nanoparticles is determined to be a = 0.5429 nm, which is slightly smaller than the value for bulk Si. From the widths of the (111), (200) and (311) peaks, a mean crystallite size of d_{cryst} ≅ 6 nm is estimated using the Scherrer formula.[21] This is in reasonable agreement with the BET result and, thus, indicates that the Si nanoparticles are single crystalline.

3.3. High Resolution Transmission Electron Microscopy (HRTEM)

Figure 6 shows an example of a HRTEM image of Si nanoparticles taken from the same batch with d_P(BET) = 5 nm of which the XRD pattern was presented in Fig. 5. Here,

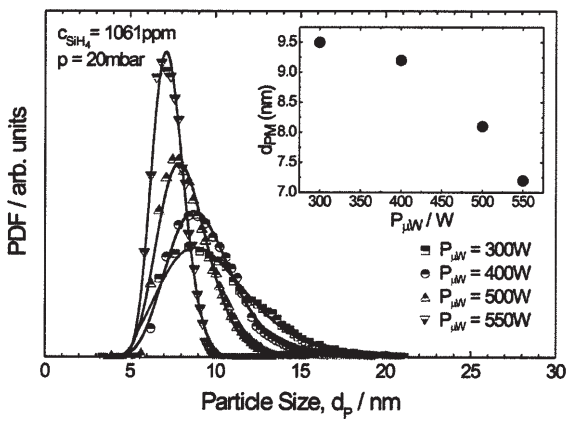

Fig. 4. Influence of the microwave power, $P_{\mu W,}$ on the particle size distribution, as determined by particle mass spectrometry. The precursor concentration of silane and the total gas pressure are c(SiH_4) = 1061 ppm and p = 20 mbar, respectively. The insert shows the resulting mean particle size d_{PM} as a function of $P_{\mu W}$.

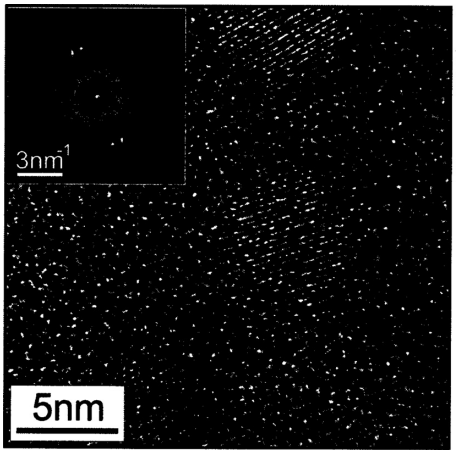

Fig. 6. HRTEM micrograph of gas-phase prepared Si nanoparticles with a BET diameter of d_P(BET) = 5 nm deposited onto amorphous carbon films. The (111) lattice fringes of the diamond type lattice of the particles are clearly visible and give rise to the two pairs of brightest spots in the diffractogram (i.e., the fourier transform of the image) displayed in the upper left corner.

the particles were deposited onto amorphous carbon film (~10 nm) supported by a Cu grid. In order to deposit the particles onto the TEM grid, the particle powder was dispersed in ethanol with the aid of sonification, and the TEM grid was then dipped into the dispersion and subsequently dried. The coverage of the carbon film was very low, and as a consequence, electron diffraction did not yield any valuable results. Due to the small atomic mass of Si, the (amplitude) contrast of the nanoparticles against the background of the carbon carrier film is poor. However, the phase contrast arising from the (111) lattice fringes of the particles is clearly visible. From the diffractogram, as obtained by Fourier transformation of the original image (cf. insert in the upper left corner of Fig. 6), the (111) lattice spacing of the nanoparticle was determined. From this image and a variety of other HRTEM micrographs, values of $d_{111} = 0.302$ nm, $d_{22} = 0.188$ nm and $d_{311} = 0.161$ nm were measured, which are all somewhat smaller than the respective lattice spacings in bulk Si. This is in general agreement with the results obtained from the XRD investigations, although these HRTEM measurements are less precise, since they are uncalibrated. However, such deviations from the bulk lattice constants are typical for nanoparticles and depend crucially on their environment.[16, 22] As determined from HRTEM images, the particle sizes are $d_P = 5$ to 7 nm and, thus, again in agreement with the BET results. All observed particles were found to be single crystalline. Intra-particle twinning or polycrystalline particles were not observed.

3.4. Electron Energy Loss Spectroscopy (EELS)

In order to examine the possible surface oxidation of the Si nanoparticles, EELS measurements were conducted. The electron energy loss spectrum was measured within a circular area with a diameter of 180 nm on the TEM grid. The area studied contains about 20 particles (due to the low contrast, no image is shown here). In Fig. 7, the resulting EEL spectrum (topmost solid line) of the as-deposited particles is presented. The intensity is plotted as function of the energy loss ΔE in the vicinity of the Si K-edge (ΔE = 99 eV). Due to the small number of Si nanoparticles within the investigated area, some noise is superimposed to the signal. The second spectrum displayed in Fig. 7 was obtained under identical condition, but the sample has been previously exposed to an oxygen plasma for $\tau = 10$ s. For comparison, two reference EEL spectra for pure Si and SiO_2[23] are also shown. The spectrum obtained from the as-deposited sample differs significantly from the spectrum of the plasma treated sample. Whereas in the first case, the EEL signal rises at the onset of the edge and increases to a broad maximum before decreasing again with increasing ΔE, the plasma treated sample displays a sharp cusp and two subsequent pronounced minima toward larger energy losses. From a comparison with the Si and SiO_2 reference

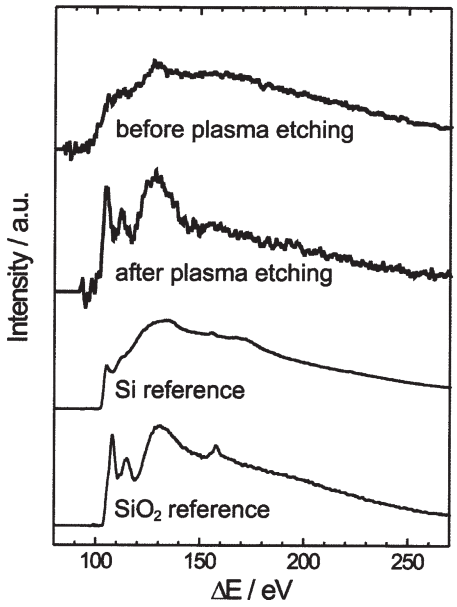

Fig. 7. Electron energy loss spectra in the vicinity of the Si K-edge, as obtained from Si nanoparticles deposited onto amorphous carbon. The spectra are taken within a circular area with a diameter of 180 nm. The topmost spectrum originates from as-deposited particles, whereas the second spectrum is obtained after exposing the sample to an oxygen plasma for 10 s. For comparison, we show reference EELS data for Si and SiO_2. See text for details.

data, it is obvious that the as-deposited nanoparticles are predominantly pure Si, whereas the plasma treatment results in a thorough oxidation of the particles to SiO_2. Together, with the structural results obtained from the HRTEM investigations, the EELS data show that the produced particles are Si. The existence of an (amorphous) surface oxide layer, which is often observed in gas-phase prepared Si nanoparticles, cannot be excluded.

3.5. Fourier Transform Infrared Spectroscopy (FTIR)

The FTIR spectrum of Si nanoparticles with d_P(BET) = 5 nm is shown in Fig. 8 (same sample as in Figs. 5 to 7). A variety of more or less pronounced absorption bands (i.e., minima in the transmittance signal) can be seen from the spectrum. These absorption bands can be assorted in three groups. The bands located at wave numbers $k = 1625$ cm^{-1} and $k = 942$ cm^{-1} (labelled with solid squares) are attributed to O-H and Si-OH vibrations in surface-bound hydroxyl groups, respectively. The absorption bands at wave numbers $k = 2248$ cm^{-1}, $k = 1071$ cm^{-1}, $k = 981$ cm^{-1} and $k = 464$ cm^{-1} (labelled with half-filled circles) indicate a (partial) surface oxidation of the Si nanoparticles.[24] This is somewhat striking in case of the absorption band at $k = 2248$ cm^{-1}, which represents a Si-H vibration. However, in previous investigations,[12, 25] this band had been attributed to a Si-H vibration, where the

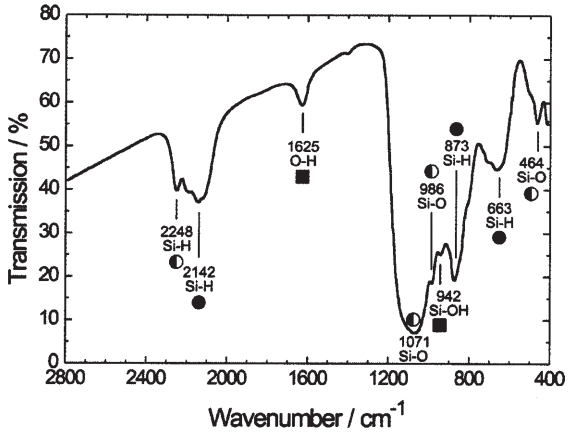

Fig. 8. Fourier transform infrared (FTIR) spectrum of Si nanoparticles with a BET diameter of d_P(BET) = 5 nm. The relative transmission is given as a function of the wave number. See text for details.

Si atom is bound via an O atom to the Si surface (*H-Si*-O-Si_{bulk}). Thus, like the three other absorption bands of this group, it provides evidence for a certain surface oxidation of the Si particles. The IR-absorption bands at $k = 1071$ cm^{-1} and $k = 981$ cm^{-1} are strongly shifted toward lower wave numbers, as compared to the LO and TO modes of amorphous SiO_2, which are located at 1250 cm^{-1} (LO) and 1090 cm^{-1} (TO). There are two possible explanations for this effect. First, it may originate from a confinement effect in ultrathin films ($t < 5$ nm),[26] and second, it may be due to an understoichiometric oxidation of silicon (SiO_x, with $x < 2$).[27] Since the magnitude of the observed shifts is far larger than what can be expected from reducing the oxide layer thickness,[26] the red shifts are attributed to an understoichiometric oxidation. Finally, the bands at $k = 2142$ cm^{-1}, $k = 873$ cm^{-1} and $k = 663$ cm^{-1} (labelled with solid circles) represent Si-H vibrations at the Si surface[28] and, thus, show that the particles are partially covered with hydrogen. This provides further confirmation for chemically bound H atoms on the surface of the Si nanoparticles. From the fact that the intensities of the Si-H bands at $k = 2142$ cm^{-1} and at $k = 873$ cm^{-1} are considerably large with respect to the Si-O bands at $k = 1071$ cm^{-1} and at $k = 986$ cm^{-1} (which exhibit high oscillatory strengths), it is deduced that the particle surfaces are only partially oxidized, most probably due to contact with air after the microwave preparation procedure. This is in good agreement with the EEL spectra of these particles, which also showed a predominant signature of Si rather than of SiO_2 (cf. Fig. 7).

4. CONCLUSION

The preparation of high purity Si nanoparticles by means of microwave induced electrical discharge dissociation of silane (SiH_4) in a low pressure flow reactor is reported. Varying the precursor concentration, the pressure or the microwave power, the mean particle size can be adjusted in the range 6 nm $\leq d_P \leq$ 11 nm. Structural investigations utilizing XRD and HRTEM show that the particles are single crystalline. EELS and FTIR measurements provide evidence that the volume of the particles is pure silicon. The particle surface is both partially covered with an ultrathin amorphous SiO_x layer ($x \leq 2$) and partially hydrolyzed. However, since all structural and chemical investigations were conducted *ex situ*, the observed surface oxidation may well occur only after exposing the particles to ambient air.

Very recent experiments have shown that the employed preparation method allows for *p*-type doping of the Si nanoparticles with boron by using di-boran (B_2H_6) as additional precursor material.[29] According investigations for *n*-type doping with phosphor are currently in progress.

Acknowledgments: Financial support by the Deutsche Forschungsgemeinschaft (DFG) and the DEGUSSA company is gratefully acknowledged.

References and Notes

1. L. T. Canham, *Appl. Phys. Lett.* 57, 1046 **(1990)**.
2. V. Lehman and U. Gösele, *Appl. Phys. Lett.* 58, 856 **(1990)**.
3. H. Takagi, H. Ogawa, Y. Yamazaki, A. Ishizaki, and T. Nakagiri, *Appl. Phys. Lett.* 56, 2379 **(1990)**.
4. A. G. Cullis and L. T. Canham, *Nature* 353, 335 **(1991)**.
5. L. N. Dinh, L. L. Chase, M. Balooch, W. J. Siekhaus, and F. Wooten, *Phys. Rev. B* 54, 5029 **(1996)**.
6. T. van Buren, L. N. Dinh, L. L. Chase, W. J. Siekhaus, and L. J. Terminello, *Phys. Rev. Lett.* 80, 3803 **(1998)**.
7. A. G. Cullis, L. T. Canham, and P. D. J. Calcott, *J. Appl. Phys.* 82, 909 **(1997)**.
8. G. Ledoux, O. Guillois, D. Porterat, C. Reynaud, F. Huisken, B. Kohn, and V. Paillard, *Phys. Rev. B* 62, 15942 **(2000)**.
9. T. Yoshida, Y. Yamada, and T. Orii, *J. Appl. Phys.* 83, 5427 **(1998)**.
10. J. M. Martínez-Duart and R. J. Martín-Palma, *Phys. Stat. Sol. B* 232, 81 **(2002)**.
11. F. Huisken, H. Hofmeister, B. Kohn, M. A. Laguna, and V. Paillard, *Appl. Surf. Sci.* 154, 305 **(1999)**.
12. H. Wiggers, R. Starke, and P. Roth, *Chem. Eng. Technol.* 24, 261 **(2001)**.
13. H. Hofmeister, P. Ködderitzsch, and J. Dutta, *J. Non-Crystalline Solids* 232, 182 **(1998)**.
14. J. Dutta, W. Basca, and Ch. Hollenstein, *J. Appl. Phys.* 77, 3729 **(1995)**.
15. C. Courteille, J.-L. Dorier, J. Dutta, Ch. Hollenstein, A. A. Howling, and T. Stoto, *J. Appl. Phys.* 78, 61 **(1995)**.
16. H. Hofmeister, F. Huisken, and B. Kohn, *Eur. Phys. J. D.* 9, 137 **(1999)**.
17. M. J. Caldas, *Phys. Stat. Sol. B* 217, 641 **(2000)**.
18. L. Pavesi, L. dal Negro, C. Mazzoleni, G. Franzò, and F. Priolo, *Nature* 408, 440 **(2000)**.
19. P. Roth and A. Hospital, *J. Aerosol Sci.* 25, 61 **(1994)**.
20. C. G. Granqvist and R. A. Buhrman, *J. Appl. Phys.* 47, 2200 **(1976)**.
21. B. E. Warren, *X-ray Diffraction*, Dover Publications, Inc., New York 253 **(1969)**.

22. B. Rellinghaus, S. Stappert, E. F. Wassermann, H. Sauer, and B. Spliethoff, *Eur. Phys. J. D.* 16, 249 **(2001)**.
23. O. L. Krivanek and C. C. Ahn, Gatan EELS Atlas.
24. H. Zhang, A. Wei, S. Liu, W. Wang, D. Chen, L. Liang, and K. Chen, *Thin Solid Films* 368, 315 **(2000)**.
25. T. M. Kramer, W. E. Rhine, and H. K. Bowen, *Adv. Ceram. Mater.* 3, 244 **(1988)**.
26. N. Nagai, K. Terada, Y. Muraji, H. Hashimoto, T. Maeda, Y. Maeda, E. Tahara, N. Tokai, and A. Hatta, *J. Appl. Phys.* 91, 4747 **(2002)**; R. A. B. Devine, *Appl. Phys. Lett.* 68, 3108 **(1996)**.
27. A. Borghesi, A. Piaggi, A. Sassela, A. Stella, and B. Pivac, *Phys. Rev. B* 46, 4123 **(1992)**.
28. A. von Keudell and J. R. Abelson, *Phys. Rev. B* 59, 5791 **(1999)**.
29. J. Knipping, H. Wiggers, and P. Roth, to be published.

Received: 14 October 2003. Revised/Accepted: 24 May 2004.